Clinical Cancer Research

# Expression of Vascular Endothelial Growth Factor in Ovarian Cancer Inhibits Tumor Immunity through the Accumulation of Myeloid-Derived Suppressor Cells

Naoki Horikawa, Kaoru Abiko, Noriomi Matsumura, Junzo Hamanishi, Tsukasa Baba, Ken Yamaguchi, Yumiko Yoshioka, Masafumi Koshiyama, and Ikuo Konishi

## Abstract

**Purpose:** High VEGF expression in ovarian cancer is an unfavorable prognostic factor. However, the role of VEGF in tumor immunity remains unclear. Here, we examined the impact of VEGF on local immunity, including induction of myeloid-derived suppressor cells (MDSC), in ovarian cancer.

**Experimental Design:** High-grade serous ovarian cancer (HGSOC) cases were analyzed by gene expression microarray and IHC for VEGF, CD8, and CD33. VEGF receptor (VEGFR) 1 and VEGFR2 expression levels on MDSCs were analyzed in a mouse model, and the direct effects of VEGF-A on MDSC expansion were investigated. $Gr1^+$ MDSCs and lymphocyte frequencies were analyzed in control tumors and tumors derived from cells harboring short hairpin RNA targeting Vegf-a. In addition, the therapeutic effects of anti-Gr-1 antibodies were examined.

**Results:** Microarray analysis revealed the upregulation of several myeloid cell chemoattractants and the downregulation of lymphocyte-related pathways in cases with high VEGF expression. In immunohistochemical analysis, VEGF expression in peritoneal dissemination correlated with MDSC infiltration. Cases with high MDSC infiltration, which was inversely correlated with intratumoral $CD8^+$ T-cell infiltration, exhibited shorter overall survival. In a mouse model, intratumoral MDSCs expressed both VEGFR1 and VEGFR2. MDSC migration and differentiation were augmented by VEGF signaling. Vegf-a knockdown in tumor cells resulted in decreased MDSC infiltration and increased $CD8^+$ T-cell infiltration. Moreover, treatment with anti-Gr-1 antibodies delayed the growth of control tumors, whereas Vegf-a-knockdown tumors were unaffected by anti-Gr-1 antibody treatment.

**Conclusions:** VEGF expression in ovarian cancer induced MDSCs, inhibited local immunity, and contributed to poor prognosis. *Clin Cancer Res; 23(2); 587–99. ©2016 AACR.*



## Introduction

Epithelial ovarian cancer represents the most lethal malignancy arising in the female genital tract, as most patients are diagnosed at an advanced stage with severe peritonitis carcinomatosa (1). Despite advancements in chemotherapy and surgical treatments, patient prognosis has not improved over the last few decades (2). Cytoreductive surgery followed by adjuvant chemotherapy using platinum cytotoxic agents is the standard therapy for advanced ovarian cancer. However, most patients relapse via peritoneal dissemination and often develop chemotherapeutic resistance (3). The progression of peritoneal dissemination directly leads to poor prognosis and impaired quality of life due to the pool of massive tumor ascites. Thus, new treatment strategies for controlling peritoneal dissemination are urgently required.

One major mechanism of solid tumor growth is the acquisition of immune evasion capacity of tumor cells (4) via the induction of cells with immunosuppressive properties such as regulatory T cells, M2 macrophages, and myeloid-derived suppressor cells (MDSC) or the expression of inhibitory molecules such as programmed cell death-ligand 1 (PD-L1) that comprises immune checkpoints (5–8). We have reported that in advanced ovarian cancer, the blockade of PD-1/PD-L1 signaling enhanced the immune response in association with $CD8^+$ T-cell infiltration (9, 10) and exerts antitumor effects (11). Patients with the immunoreactive subtype of high-grade serous ovarian cancer (HGSOC), as demonstrated by gene expression profile classifications, exhibit improved survival relative to that of patients with other subtypes (12–14). Similarly, patients with higher $CD8^+$ T-cell numbers in the tumor epithelium exhibit better prognoses (9, 15, 16). Collectively, these reports indicate that immune evasion is a key therapeutic target in ovarian cancer.

Most ovarian cancers express VEGF (17). VEGF-A, the most active member of the VEGF family, both promotes angiogenesis and is important for inducing the immunosuppressive microenvironment in tumors (18), as demonstrated by its effects on

Department of Gynecology and Obstetrics, Kyoto University Graduate School of Medicine, Kyoto, Japan.

**Note:** Supplementary data for this article are available at Clinical Cancer Research Online (http://clincancerres.aacrjournals.org/).

**Corresponding Author:** Kaoru Abiko, Department of Gynecology and Obstetrics, Kyoto University Graduate School of Medicine, 54 Shogoin Kawahara-cho, Sakyo-ku, Kyoto 606-8507, Japan. Phone: 817-5751-3269; Fax: 817-5761-3967; E-mail: kaoruvc@kuhp.kyoto-u.ac.jp

**doi:** 10.1158/1078-0432.CCR-16-0387

## Translational Relevance

VEGF has immunosuppressive as well as proangiogenic functions, yet the impact of VEGF on local immunity and the detailed mechanisms of its role in immune suppression in the tumor microenvironment remain unclear. Thus far, few studies using clinical samples have been performed. MDSCs represent a major component of the tumor immune escape mechanism although additional studies of this process from a clinical standpoint are required. Here, we show that VEGF inhibits $CD8^+$ T-cell activity in ovarian cancer through MDSC recruitment to tumor sites and contributes to poor prognoses. Furthermore, MDSCs induced by VEGF possessed stronger immunosuppressive properties than other MDSCs, and MDSC-targeted treatment was effective against VEGF-expressing tumors in a mouse model. Collectively, our data suggested that the MDSCs induced through VEGF signaling play important roles in tumor immune evasion in ovarian cancer, and that targeting of VEGF-induced MDSCs represents a promising treatment for ovarian cancer.

inhibition of dendritic cell maturation and expansion of regulatory T cells via VEGF-A/VEGF receptor (VEGFR) 2 signaling in tumor-bearing mice (19). However, the effects of VEGF-A on antitumor immunity in ovarian cancer are still unknown. MDSCs, which function as immunosuppressive factors in the tumor microenvironment (7), are defined as a heterogeneous population composed of myeloid lineage cells at various stages of differentiation that expand in the blood, lymphatic organs, and tumor sites (20–22). MDSCs have many functions including promotion of angiogenesis and tumor invasion in addition to immune suppression (23–25); however, their roles in the tumor microenvironment are not fully understood, and the clinical significance of MDSCs during ovarian cancer progression is unknown. In a study using nontumor bearing mice, VEGF has been shown to accumulate MDSCs through VEGF-A/VEGFR2 signaling (26). Therefore, in this study, we aimed to clarify the association between VEGF-A and MDSCs using ovarian cancer mouse models and clinical samples and to further demonstrate the roles of MDSCs in tumor immunity.

## Materials and Methods

### Immunohistochemical analysis of ovarian cancer cases

Surgical specimens from patients with HGSOC who underwent primary surgery at Kyoto University Hospital between 1996 and 2014 were collected after approval of the study protocol by the Institutional Ethical Committee. We selected 56 advanced cases (48 stage III cases and 8 stage IV cases) for which paired samples of the primary site and peritoneal dissemination could be evaluated. The relevant clinical data were collected by retrospective review of patient files. Patients receiving chemotherapy or radiation prior to surgery were excluded. Only cases in which tissues from both ovarian and peritoneal tumors were available from the same operation were included. Immunostaining was performed using the streptavidin–biotin–peroxidase method as described previously (10). For VEGF, CD4, CD8, and CD33, the samples were incubated with rabbit anti-VEGF polyclonal antibodies (Abs; ab46154, 1:200 dilution; Abcam), rabbit anti-CD4 Abs (clone SP35, 1:100 dilution; Cell-Marque), mouse anti-CD8 Abs (clone C8/144B, 1:100 dilution; Nichirei Biosciences), and mouse anti-CD33 mAbs (clone PWS44, 1:200 dilution; Leica Biosystems).

### Immunohistochemical evaluation

Samples were classified according to the intensity of VEGF staining and scored as follows: 0, negative; 1, very weak; 2, moderate; and 3, strong expression as shown in Fig. 1A. Samples with heterogeneous staining were scored on the basis of the intensity in the largest stained area. Samples with less than 50% of tumor cell staining were considered negative. Cases with scores of 0/1 and 2/3 were defined as VEGF low- and high-expression groups, respectively. Tumor-infiltrating immune cells were evaluated as described previously (27). Briefly, intratumoral $CD33^+$ cells were counted at 200× magnification, and $CD4^+$ and $CD8^+$ cells were counted at 400× in five different microscopic fields with the most abundant infiltration, and the average number was calculated.

### HGSOC gene expression microarray analysis

HGSOC specimens were obtained from 32 patients who underwent primary surgery at Kyoto University Hospital between 1997 and 2012 and were prepared for gene expression microarray analysis. Data were previously deposited in the Gene Expression Omnibus (accession numbers: GSE 39204 and GSE55512; refs. 10, 28). Total RNA expression was analyzed using the Human Genome U133 Plus 2.0 Array (Affymetrix), and robust multi-array averaging normalization was performed using R (version 2.15.1) software (https://www.r-project.org/). Two groups were defined on the basis of VEGF staining of relevant samples. Probes showing expression values with SDs greater than 0.2 across all samples were filtered, and the Samroc method was used for statistical analysis as described previously (29). Differentially expressed genes were sorted in ascending order by rank-fold change, and up- or downregulated genes ($P$ values $< 0.01$) were defined as the VEGF signature.

Gene-set enrichment analysis (GSEA) was performed to evaluate pathway activation using the c5.all.v.3.1.format (http://software.broadinstitute.org/gsea/msigdb). A variant of GSEA, ssGSEA (30), was performed using R to evaluate VEGF signature activity in HGSOC samples.

### Cell lines and tumor models

The OV2944-HM-1 (HM-1) mouse ovarian cancer cell line was purchased from RIKEN BioResource Center in January 2003 and cultured as described previously (31). The ID8 mouse ovarian cancer cell line and its *Vegf-a*–overexpressing derivative were kindly provided by Dr. Katherine Roby (The University of Kansas Medical Center, Kansas City, KS) (32) in September 2009. These cells were cultured and maintained in RPMI1640 (Invitrogen) supplemented with 10% FBS, 100 U/mL penicillin, and 100 g/mL streptomycin in an atmosphere containing 5% $CO_2$ at 37°C. These cells were proven to have immunogenicity and are often used for immunologic research (28, 31). Throughout this study, we used ID8 and HM-1 cell lines after passaging for fewer than 30 times. All cell lines were regularly tested for mycoplasma contamination. Authentication of these cells with short tandem repeat analysis was not performed because they were derived from mice.

HM-1 sh*Vegf-a* and HM-1-control cell lines were generated by lentiviral transfection with short hairpin RNAs (shRNA) as described previously (11). Female C57BL/6 (B6) mice were purchased from CLEA Japan and B6C3F1 (C57BL6 × C3/He F1) mice were purchased from Charles River Japan. Animal experiments were approved by the Kyoto University Animal Research Committee, and animals were maintained under specific pathogen-free conditions. A total of $5 \times 10^6$ ID8-Vegf or ID8 control cells were inoculated intraperitoneally into B6 mice, and $1 \times 10^6$ HM-1 sh*Vegf-a* cells or HM-1control cells were inoculated subcutaneously into the right flank or injected into the abdominal cavity of B6C3F1 mice. Anti-Gr-1 antibody treatment was initiated 4 days after tumor cell inoculation and administered intraperitoneally at 150 μg/mouse twice a week as described previously (33). Subcutaneous tumor size and body weight were measured twice a week and tumor volumes were calculated as volume = LD × $SD^2$ × 0.4, where LD is the long diameter (mm) and SD (mm) is the short diameter of the tumor (34).

### Flow cytometry

For human samples, ascitic cells were collected from patients with HGSOC who underwent abdominal surgery. For murine samples, mice with tumor formation were euthanized by $CO_2$ gas inhalation and their spleens, femurs, tibias, and tumors were collected. Cells were stained with the following Abs for 30 minutes at 4°C: anti-human CD11b (clone M1/70), anti-human CD33 (clone WM53), anti-human VEGFR2 (clone ES8-20E6), anti-human/mouse ARG1, anti-mouse CD4 (clone RM4-5), anti-mouse CD8a (clone 53-6.7), anti-mouse CD45 (clone 30-F11), anti-mouse Gr-1 (clone RB6-8C5), and anti-mouse CD11b (clone M1/70). For ARG1 intracellular staining, a BD Cytofix/Cytoperm Fixation/Permeabilization Kit (BD Biosciences) was used. Nonviable cells were stained with 7-amino-actinomycin D (AAD) staining solution or DAPI solution and gated out. Matched isotype Abs were used as controls. Data were acquired using a MACS Quant (Miltenyi Biotec) or FACSCalibur (BD Biosciences) and analyzed using MACS Quantify (Miltenyi Biotec) or Cell Quest Pro software (BD Biosciences).

### Immunohistochemical analysis of mouse tumors

Mouse tumor cryosections (6-μm thick) were stained with anti-CD4 (clone H129.19; BD Pharmingen/BD Biosciences), anti-CD8 (clone YTS169.4; Abcam), anti-CD11b (clone M1/70; BioLegend), or anti-Gr-1 (clone RB6-8C5; BD Pharmingen) Abs, as described previously (31). The numbers of $CD4^+$, $CD8^+$, $CD11b^+$, and $Gr\text{-}1^+$ cells infiltrating into ID8 omental tumors were evaluated. For immunofluorescence staining, anti-VEGFR1 (clone Y103; Abcam), anti-VEGFR2 (clone 55B11; Cell Signaling Technology), anti-phospho-VEGFR1 (clone Tyr1213; Millipore), and anti-phospho-VEGFR2 (clone Tyr1175; Cell Signaling Technology) Abs were used as primary Abs. Anti-IgG labeled with AlexaFluor 488 (Abcam) and AlexaFluor 594 (Abcam) was used as the secondary antibody. Nuclei were stained with DAPI solution (Dojindo). Fluorescence images were captured using a Keyence BZ-X700 microscope (Keyence).

### MDSC generation assay

To generate MDSCs, bone marrow cells were harvested from the femurs and tibias of naïve B6 mice. Bone marrow cells ($1 \times 10^6$) were cultured in RPMI1640 supplemented with 10% FBS, 10 ng/mL GM-CSF, 10 ng/mL IL4, and 50 μmol/L β-mercaptoethanol in the presence of 30% v/v tumor supernatant from confluent ID8 cells in 24-well plates. Recombinant VEGF (rVEGF; PeproTech) at 10 μg/mL or anti-VEGF antibody (B20-1.1; Genentech) at 10 μg/mL was added to each well. The cultures were maintained at 37°C in an atmosphere containing 5% $CO_2$ for 5 days. Medium containing each substance was replaced on day 3, and the cells were collected on day 5 for flow cytometric analysis.

### MDSC suppression assay

The purified MDSC ($CD11b^+Gr1^+$) population was sorted from ID8 tumor ascites using auto magnetic-activated cell sorting (autoMACS Pro separator; Miltenyi Biotec) according to the manufacturer's protocol. An aliquot of the $Gr1^+$-sorted cells was stained with anti-CD11b Abs and analyzed by flow cytometry to ensure the purity (>90%) of the $CD11b^+Gr1^+$ cells. Carboxyfluorescein succinimidyl ester (CFSE; 10 μmol/L) was added to suspensions ($1 \times 10^7$ cells/mL) of T cells separated from splenocytes of a wild-type C57BL/6 mouse using a mouse Pan-T-cell isolation kit (Miltenyi Biotec). Sorted MDSCs or recombinant VEGF were added to CFSE-labeled T cells at different ratios, harvested in 96-well plates, and activated with Dynabeads Mouse T-activator CD3/28 (VERITAS) for 72 hours at 37°C. T-cell proliferation was evaluated by flow cytometry.

### Reverse transcription PCR and real-time quantitative PCR

Total RNA was extracted from cells and frozen tissues using an RNeasy Mini Kit (Qiagen). A transcriptor High Fidelity cDNA Synthesis Kit was used for cDNA synthesis (Roche Diagnostics). For reverse transcription (RT)-PCR, the cDNAs were amplified using a thermal cycler. Real-time quantitative PCR was carried out by amplification of the target genes and *Gapdh* mRNA as a reference gene using a Light Cycler 480-II (Roche Diagnostics). The primers used in these experiments are listed in Supplementary Table S5. Relative target gene expression was estimated by dividing the threshold cycle ($C_t$) value of the target gene by the $C_t$ value for *Gapdh* mRNA.

### Immunoblotting and ELISA

Immunoblotting was performed with the following primary Abs: anti-VEGF (ab46154, 1:1,000 dilution; Abcam) and anti-β-actin (1:1,000 dilution; Cell Signaling Technology). Serum was obtained from tumor-bearing mice. Serum VEGF levels were measured using a Mouse VEGF assay kit according to manufacturer's instructions (IBL).

### Granzyme B induction assay

Splenocytes ($1 \times 10^6$) were cultured with Dynabead Mouse T-activator CD3/28 (VERITAS) stimulation for 72 hours. Cells were harvested and stained for surface markers, then fixed and stained for intracellular granzyme B (1:200 dilution; eBioscience) and analyzed by flow cytometry.

### Cell proliferation assay

HM-1 or HM-1 sh*Vegf-a* cells were seeded in 96-well tissue culture plates at $1 \times 10^3$ cells/well. Water-soluble tetrazolium-8 assays were performed using Cell Count Reagent SF (Nacalai Tesque) according to the manufacturer's protocol.

### Chemotaxis assay

*In vitro* migration of MDSCs was evaluated in 24-well plates with transwell polycarbonate-permeable supports (8.0 μm; Costar Corning). MDSCs ($5 \times 10^5$; >90% $Gr1^+CD11b^+$) were plated in 100-μL MEMα in the top chambers of the inserts 30 minutes after incubation with anti-VEGFR1 Abs (10 μg/mL; R&D Systems), anti-VEGFR2 Abs (10 μg/mL; R&D Systems), or IgG control Abs, and 500 μL chemoattractant [tumor-conditioned medium (TCM) ± 10 μg/mL anti-VEGF Abs] was then added to the bottom chamber. Plates were incubated at 37°C with 5% $CO_2$ for 2–3 hours, and the number of MDSCs in the bottom compartment was counted using Acubright counting beads (Life Technologies). To obtain the TCM, supernatants were harvested from confluent cultures of HM-1 or HM-1 sh*Vegf-a* cells cultured in MEMα containing 10% serum.

### Statistical analysis

Results are shown as the average ± SEM as appropriate. Group comparisons were performed using Mann–Whitney *U* tests and Fisher exact test. Univariate prognostic analysis was performed using log-rank tests, and multivariate analysis was performed using Cox proportional hazards tests. All statistical analyses were performed using GraphPad Prism 6 and Rcmdr software (http://www.rcommander.com/). Differences with $P$ value <0.05 were considered significant.

## Results

### High VEGF expression in HGSOC was associated with suppressed immune-response signaling

To determine the biological signals affected by VEGF expression in HGSOC clinical samples, we first analyzed the results from a gene expression microarray of resected tumor tissues. These samples were classified into four groups based on the VEGF expression as determined by immunostaining of the relevant paraffin-embedded sections (Fig. 1A). Samples with scores of 0/1 or 2/3 were assigned to the VEGF-low and -high groups, respectively (Supplementary Table S1). Among the upregulated genes in the VEGF-high group, *CXCL1*, *CXCL2*, and *CXCL5* are reported to encode myeloid cell chemoattractants, and *IL6* and *PTGS2* encode immunosuppressive molecules (Fig. 1B). Pathway analysis revealed that in addition to angiogenesis, the epithelial-to-mesenchymal transition pathway and several invasion-related pathways containing matrix proteases were upregulated in the VEGF-high group (Fig. 1B; Supplementary Table S2), whereas several immune-related pathways, such as T-cell and lymphocyte activation, were significantly downregulated (Fig. 1C; Supplementary Table S2).

For confirmation, we defined differentially expressed genes as the VEGF signature (Supplementary Table S3) and applied this signature to ovarian cancer microarray datasets from The Cancer Genome Atlas (TCGA), in which four molecular subtypes (differentiated, immunoreactive, mesenchymal, and proliferative) had been determined (12). VEGF signature scores for each sample were calculated by ssGSEA; significantly lower scores were observed for the immunoreactive group ($P <$ 0.001; Fig. 1D). Likewise, analysis of VEGF signature scores for our clinical samples, which were classified on the basis of microscopic examination as described previously (13), revealed that cases with strong VEGF staining intensity had significantly higher VEGF signature scores than those with weak staining (Supplementary Fig. S1A). In addition, immunoreactive type had significantly lower scores than the mesenchymal and differentiated types (Supplementary Fig. S1B). These data suggested that high VEGF expression within HGSOC inhibited lymphocyte-related signaling and promoted tumor angiogenesis and invasion.

### VEGF expression and MDSC infiltration in HGSOC peritoneal dissemination were associated with unfavorable prognoses

Because both myeloid cell chemoattractants and immunosuppressive molecules were highly expressed in the VEGF-high group, we assumed that MDSCs, as immunosuppressive cells, would contribute to VEGF-induced immune suppression. The progression of HGSOC peritoneal dissemination is directly related to poor prognosis; thus, investigation of local immunity in peritoneal dissemination and the primary tumor is important. To examine the association of tumor VEGF expression with various immune cell fractions, we performed IHC for VEGF, CD33 (an MDSC marker), CD4, and CD8 in paired surgical specimens of primary ovarian tumors and peritoneal disseminations. Among 56 patients, 34 primary tumors (60.7%; Table 1) were defined as VEGF-high as were 39 peritoneal disseminations (69.6%; Table 1). There was no correlation of VEGF expression between primary and metastatic tumors (data not shown). Patients with VEGF-high staining showed significantly shorter overall survival ($P < 0.05$; Fig. 2A) and shorter progression-free survival (Supplementary Fig. S2A) than those with VEGF-low staining; however, no difference in overall survival was observed with VEGF-high primary tumor staining ($P = 0.43$). VEGF-high staining in peritoneal dissemination was associated with suboptimal surgery ($P <$ 0.05; Table 1), suggesting that VEGF induced invasive tumor cell characteristics and caused difficulties in tumor resection.

Next, we examined the impact of $CD33^+$ cell frequency on patient survival. $CD33^+$ cells were heterogeneously distributed and preferentially localized at the tumor stroma rather than the epithelium (Fig. 2B). Patients with high infiltration of $CD33^+$ cells in peritoneal dissemination showed significantly shorter overall survival ($P < 0.001$; Fig. 2C), and progression-free survival ($P < 0.01$; Supplementary Fig. S2B) than those with low infiltration, whereas no difference was observed in those with high infiltration in the primary tumor ($P = 0.36$; Fig. 2C). There was no correlation in infiltration of $CD33^+$ cells between primary and metastatic tumors (data not shown). Multivariate analysis using the Cox regression hazard model revealed that infiltration of $CD33^+$ cells in peritoneal dissemination might serve as a prognostic factor equivalent to complete surgical resection for overall survival [relative risk (RR), 3.023; 95% confidence interval (CI), 1.140–8.015; $P < 0.05$; Supplementary Table S4].

### VEGF expression in peritoneal dissemination correlated with MDSC infiltration

VEGF scores in peritoneal dissemination were significantly correlated with $CD33^+$ ($r = 0.41$, $P = 0.0015$; Fig. 2D) but not with $CD4^+$ cell infiltration (data not shown). Notably, $CD8^+$ and $CD33^+$ cell infiltration were inversely correlated ($r = -0.29$, $P =$ 0.033; Fig. 2E). Furthermore, patients with high $CD8^+$ cell infiltration in the tumor epithelium exhibited longer survival ($P =$ 0.0034; Supplementary Fig. S2C), as previously reported in primary sites (10). Patients with high CD8/CD33 ratios showed

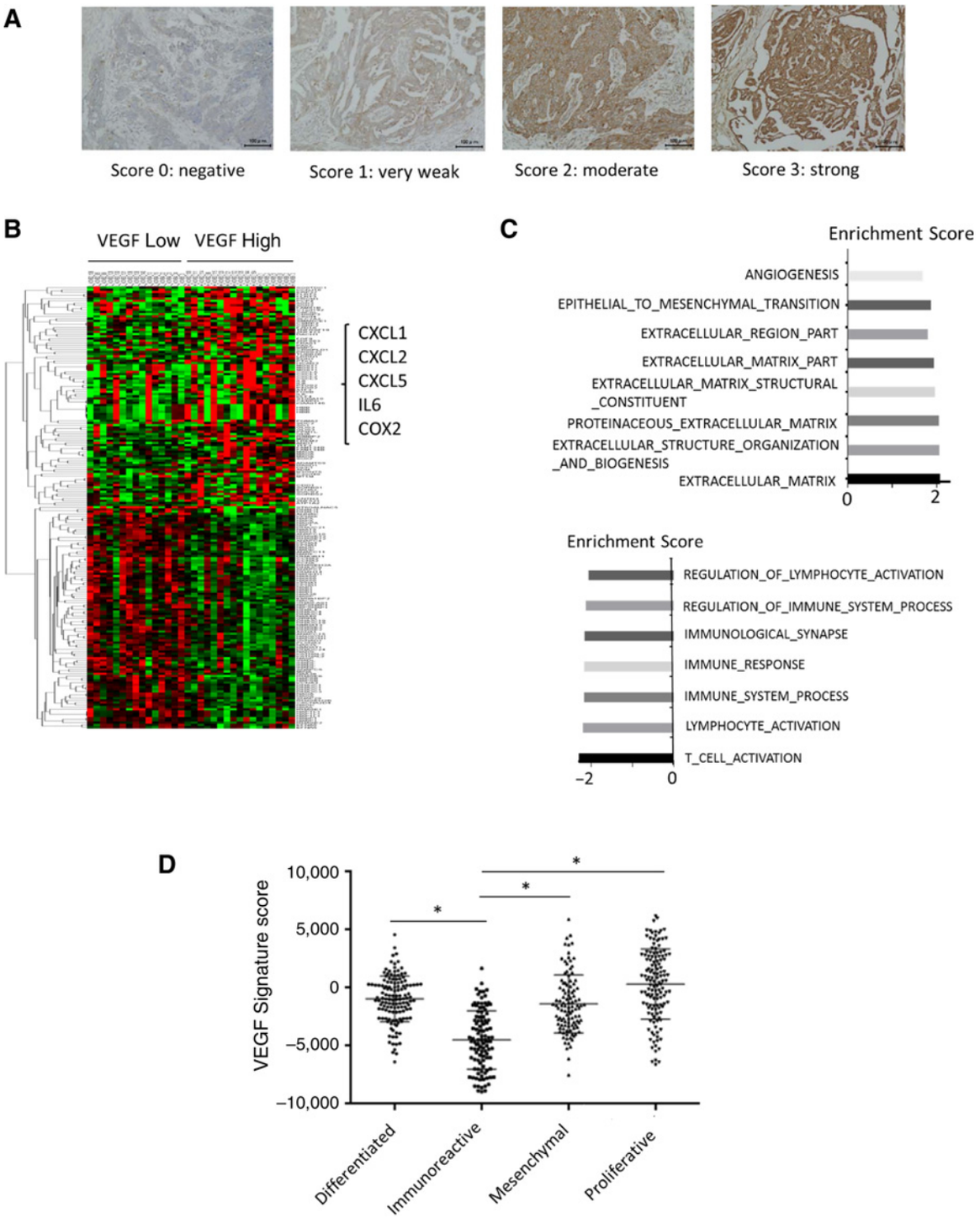


**Figure 1.**

High expression of VEGF contributes to immune suppression in HGSOC. **A,** Classification of HGSOC according to the intensity of VEGF staining. Cases with scores of 0/1 were assigned to the VEGF-low group, whereas scores of 2/3 were assigned to the VEGF-high group. Scale bar, 100 μm. **B,** Expression microarray analysis of HGSOC clinical samples ($n = 32$). Heatmap of discriminating genes for VEGF expression based on immunostaining are shown. **C,** Gene set enrichment analysis (GSEA) with gene ontogeny (GO) terms. Positive enrichment scores indicate significantly upregulated pathways in the VEGF-high group ($P < 0.01$), whereas negative enrichment scores indicate significantly downregulated pathways in the VEGF-high group ($P < 0.01$). **D,** VEGF signature scores of HGSOC samples in web-published TCGA datasets. The VEGF signature consists of the top 139 ranked genes discriminating VEGF expression (Supplementary Table S2). Signature scores were calculated following the method of single sample gene set enrichment analysis (ssGSEA). *, $P < 0.001$.

**Table 1.** Correlations between clinicopathologic parameters and VEGF expression in primary or metastatic tumors

| | | VEGF expression in ovary | | | VEGF expression in omentum | | |
|---|---|---|---|---|---|---|---|
| **Parameter** | **Case ($n = 56$)** | **Low** | **High** | ***P*** | **Low** | **High** | ***P*** |
| Age, years | | | | | | | |
| <55 | 21 | 7 | 14 | 0.5771 | 8 | 13 | 0.3779 |
| ≧55 | 35 | 15 | 20 | | 9 | 26 | |
| FIGO stage | | | | | | | |
| IIIb + IIIc | 48 | 18 | 30 | 0.6983 | 14 | 34 | 0.6876 |
| IV | 8 | 4 | 4 | | 3 | 5 | |
| LN metastasis | | | | | | | |
| Negative | 28 | 10 | 18 | 0.7723 | 8 | 20 | 1 |
| Positive | 20 | 8 | 12 | | 6 | 14 | |
| Distant metastasis | | | | | | | |
| Negative | 48 | 18 | 30 | 0.6933 | 14 | 34 | 0.6876 |
| Positive | 8 | 4 | 4 | | 3 | 5 | |
| Residual tumor | | | | | | | |
| Optimal | 37 | 15 | 22 | 1 | 15 | 22 | 0.0307[a] |
| Suboptimal | 19 | 7 | 12 | | 2 | 17 | |

Abbreviation: LN, lymph node.
[a]Statistically significant.

significantly longer survival than those with low CD8/CD33 ratios ($P = 0.0064$; Supplementary Fig. S2D). These results suggested that VEGF expression in peritoneal dissemination was likely correlated with $CD33^+$ cell induction and $CD8^+$ cell reduction.

### MDSCs from patient ascites inhibited T-cell proliferation

To examine whether peritoneal dissemination–associated $CD33^+$ cells suppressed T- cell function, we isolated $CD33^+$ cells from patient ascites using magnetic bead-based separation and incubated the isolated cells with proliferating T cells. The $CD33^+$ cells expressed CD11b, but did not express lineage markers including CD2, CD19, and CD56 (Supplementary Fig. S2E). HLA-DR and CD14/CD15 expression profiles showed differential patterns among samples (Supplementary Fig. S2F). Furthermore, $CD33^+$ cells in ascites expressed VEGFR2 (Supplementary Fig. S2E). The $CD33^+$ cells expressed high levels of ARG1 and markedly decreased T-cell proliferation compared with that of controls (Fig. 2F and G). Thus, $CD33^+$ cells in the tumor microenvironment suppressed T-cell function as MDSCs and were likely associated with tumor progression through suppression of antitumor immunity.

### VEGF in mouse tumors increased intratumoral MDSCs and decreased $CD8^+$ cells

To investigate the effects of VEGF expression on immune cell infiltration in peritoneal dissemination, we generated a mouse ovarian cancer dissemination model using *Vegf*-overexpressing ID8 cells, wherein elevated VEGF-A expression had been confirmed by RT-PCR and immunoblotting (Supplementary Fig. S3). Disseminated tumors were harvested 25 days after tumor inoculation when the ascites fluid was still limited, and were immunostained for CD4, CD8, CD11b, and Gr-1 (Fig. 3A). Infiltrating $CD8^+$ cells were significantly decreased in *Vegf*-overexpressing tumors, and $CD11b^+$ and $Gr\text{-}1^+$ cells were increased. In contrast, there were no differences in infiltrating $CD4^+$ cells (Fig. 3B). $Gr\text{-}1^+$ cells separated from ID8 tumor ascites inhibited T-cell proliferation in a concentration-dependent manner, whereas addition of recombinant VEGF did not affect T-cell proliferation (Fig. 3C). These results indicated that immunosuppression was not caused by the direct effects of VEGF on lymphocytes, but was mediated thorough MDSC infiltration.

### Expression of VEGFR2 on MDSCs was elevated in tumors

To examine whether VEGF-A directly affected MDSC function, we analyzed the expression of VEGFR on MDSCs. Both VEGFR1 and VEGFR2 were expressed on MDSCs in tumors (Fig. 4A); however, VEGFR2 was not expressed on splenic MDSCs (Fig. 4B). Receptor phosphorylation on intratumoral MDSCs was confirmed by immunofluorescence (Supplementary Fig. S4). Notably, the frequency of $VEGFR2^+$ MDSCs increased in tumors, whereas the proportions of $VEGFR1^+$ cells were similar across organs ($P < 0.05$; Fig. 4C), suggesting that VEGFR2, but not VEGFR1 signaling, contributed to MDSC recruitment to tumors. In addition, the frequencies of $VEGFR2^+$ subpopulations were higher in ARG1-expressing MDSCs than in ARG1-negative MDSCs (23.67% vs. 5.01%; $P < 0.05$; Fig. 4D), indicating that $VEGFR2^+$ MDSCs in tumors possessed stronger immunosuppressive properties.

### VEGF directly promoted MDSC differentiation and migration

Next, we examined the effects of VEGF-A on MDSC differentiation. The proportion of MDSCs was significantly increased by recombinant VEGF supplementation in the culture medium ($P < 0.05$; Fig. 4E, left) but significantly decreased by anti-VEGF Abs ($P < 0.05$; Fig. 4E, right), which also reduced ARG1 expression (Fig. 4F). Moreover, MDSC migration was augmented by HM-1 control TCM but attenuated by sh*Vegf-a* TCM and anti-VEGF Ab supplementation ($P < 0.05$; Fig. 4G). Pretreatment of MDSCs with anti-VEGFR2 Abs, but not anti-VEGFR1 Abs, significantly attenuated MDSC migration ($P < 0.05$; Fig. 4G), suggesting that VEGF signaling directly affected MDSC differentiation and that VEGF/VEGFR2 signals promoted MDSC recruitment to tumors.

### VEGF inhibited the functions of CTLs through MDSC accumulation and promoted tumor progression

For further confirmation, we generated a *Vegf-a*–silenced ovarian cancer cell line, HM-1 sh*Vegf-a*, confirmed by RT-PCR and immunoblotting (Supplementary Fig. S5A and S5B), and inoculated subcutaneously to syngeneic mice. Cell proliferation *in vitro* did not differ between sh*Vegf-a* and control cells (Supplementary Fig. S5C). In mice, subcutaneous sh*Vegf-a* tumors grew more slowly than control tumors (Fig. 5A). In a peritoneal dissemination model, sh*Vegf-a* tumor-bearing mice

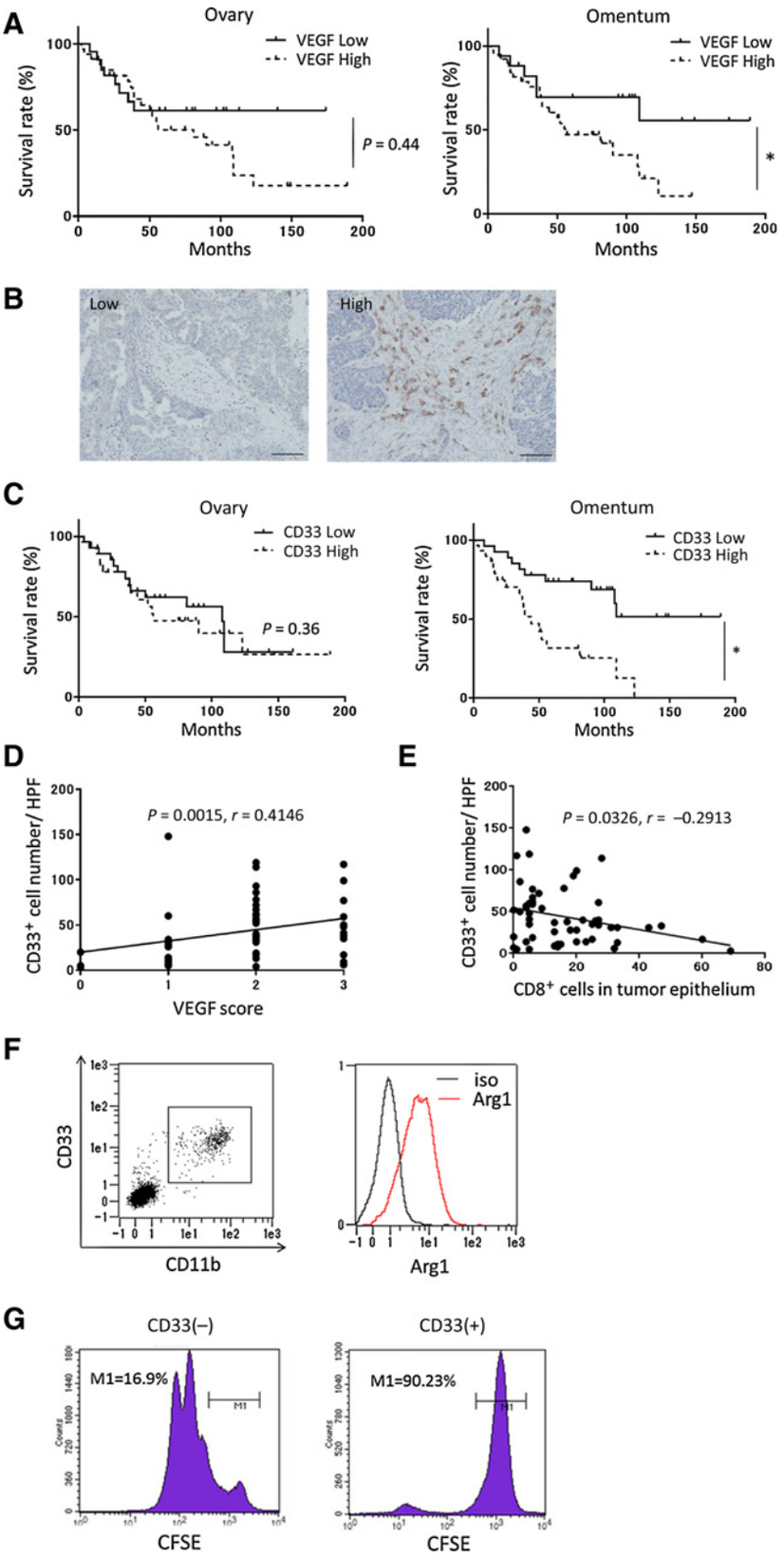


**Figure 2.**

The number of infiltrating CD33$^+$ cells correlated with VEGF expression in peritoneal dissemination. **A,** Survival analyses of patients with HGSOC ($n = 56$) according to the degrees of VEGF staining. Overall survival rates were compared between VEGF-low and VEGF-high groups either in the primary sites (left) or disseminated tumors in the omentum (right; *, $P < 0.05$). **B,** Representative IHC images for CD33 in peritoneal disseminations of HGSOC. Scale bar, 100 μm. **C,** Survival analyses of patients with HGSOC according to CD33$^+$ cell infiltration. Overall survival rates were compared between the CD33-low group and CD33-high group either in primary sites (left) or disseminated tumors in the omentum (right). *, $P < 0.005$. **D,** Correlation between infiltration of CD33$^+$ cells and VEGF expression in peritoneal dissemination. *, $P < 0.01$. **E,** Correlation between infiltration of CD33$^+$ cells and intraepithelial CD8$^+$ cells in peritoneal dissemination. **F,** Flow cytometric analysis of ARG1 expression in CD33$^+$ cells in HGSOC ascites. A dot plot is shown after exclusion of the dead cells by 7-AAD staining. CD11b$^+$ and CD33$^+$ cells were gated and analyzed for ARG1 expression. The black line shows the isotype control; the red line shows ARG1$^+$ cells. **G,** Flow cytometric analysis of the proliferation of CFSE-labeled human T cells 7 days after incubation with or without CD33$^+$ cells from HGSOC ascites.

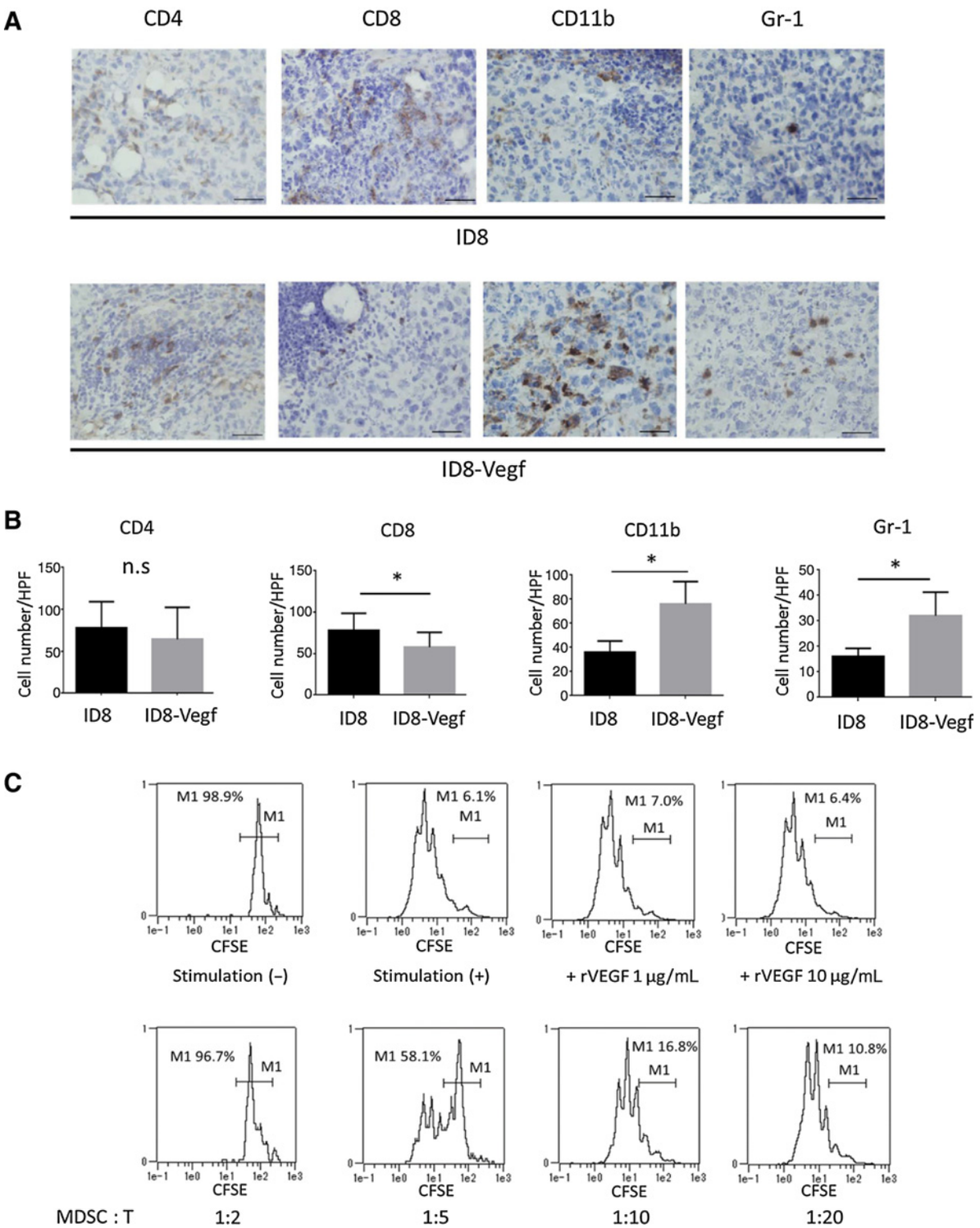


**Figure 3.**

*Vegf*-overexpressing tumors increased the infiltration of myeloid cells, whereas $CD8^+$ lymphocytes were decreased. **A,** Representative immunostaining images of ID8 or ID8-Vegf omental tumors for CD4, CD8, CD11b, and Gr-1. Scale bar, 20 μm. **B,** Analyses of the infiltration of $CD4^+$, $CD8^+$, CD11b, and $Gr\text{-}1^+$ cells within ID8 or ID8-Vegf tumors. *, $P < 0.05$. **C,** Flow cytometric analysis of the proliferation of CFSE-labeled T cells 72 hours after incubation with 1 or 10 μg/mL. Recombinant VEGF or with $Gr1^+$ cells extracted from ID8 ascites at different concentrations.

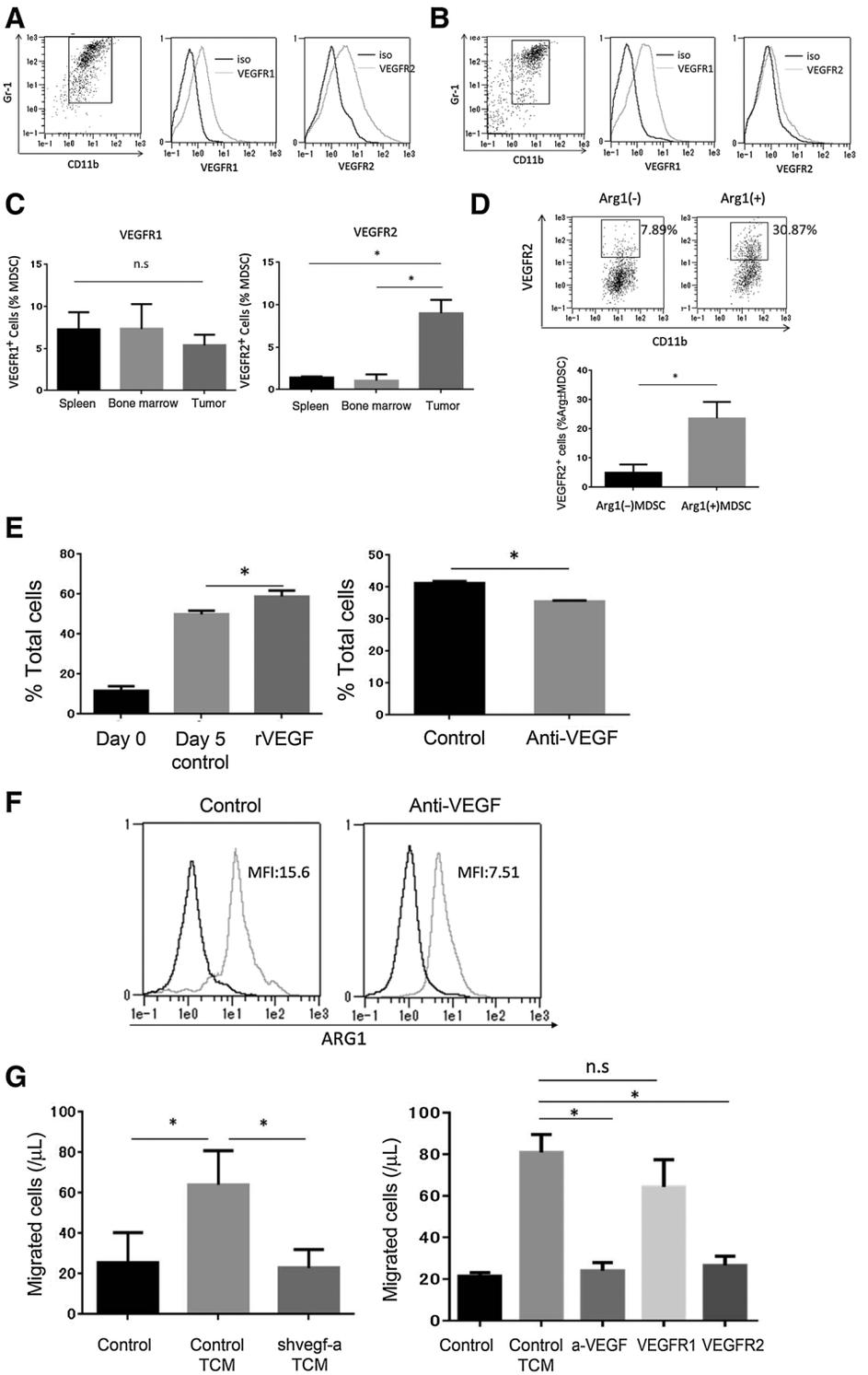


**Figure 4.**

VEGF directly induced MDSCs and recruited them to tumors. **A,** Flow cytometric analysis of VEGFR1/2 expression on MDSCs in HM-1 tumors after gating on $CD45^+$ live cells. The black line shows the isotype control; the gray line shows $VEGFR^+$ cells. **B,** Flow cytometric analysis of VEGFR1/2 expression on MDSCs in spleens from HM-1 tumor-bearing mice after gating on $CD45^+$ live cells. The black line shows the isotype control; the gray line shows $VEGFR^+$ cells. **C,** Frequencies of VEGFR1/2–positive cells as a percentage of MDSCs in the spleen, bone marrow, and tumor cells. *, $P < 0.05$. **D,** Frequencies of VEGFR2-positive cells as a percentage of ARG1-positive or -negative subpopulations of MDSCs in HM-1 tumors. *, $P < 0.05$. **E,** Flow cytometric analysis of the accumulation of tumor supernatant–derived MDSCs. Recombinant VEGF (10 μg/mL) or anti-VEGF antibody (10 μg/mL) was supplemented in the culturing medium. *, $P < 0.05$. **F,** ARG1 expression in tumor supernatants derived from MDSCs supplemented with rat IgG control or anti-VEGF antibody (10 μg/mL). The black line shows the isotype control; the gray line shows $ARG1^+$ cells. **G,** Chemotaxis assay of MDSCs in response to HM-1 or HM-1 sh*Vegf-a* cell–conditioned medium (left), or chemotaxis assay of MDSCs preincubated with control IgG, anti-VEGFR1 antibody (VEGFR1), or anti-VEGFR2 antibody (VEGFR2) in response to HM-1 cell–conditioned medium supplemented with or without anti-VEGF antibody (a-VEGF; right). TCM, tumor cell–conditioned medium. Each bar graph summarizes the data from two independent experiments. *, $P < 0.05$.

showed significantly longer survival ($P < 0.05$; Supplementary Fig. S5D and S5E). In the tumor, expression of *Vegf-a*, but not other chemoattractants for MDSCs including *CXCLs*, was decreased ($P < 0.05$; Supplementary Fig. S6). Flow cytometric analysis of the spleen and tumor demonstrated that $CD11b^+/Gr1^+$ MDSCs were significantly decreased, whereas $CD8^+$ cells were significantly increased in sh*Vegf-a* tumors ($P < 0.05$; Fig. 5B). MDSCs in HM-1 tumors exhibited significantly higher levels of ARG1 expression than those in HM-1 *shVegf-a* tumors ($P < 0.05$; Fig. 5C). Both $CD4^+$ and $CD8^+$ cells in

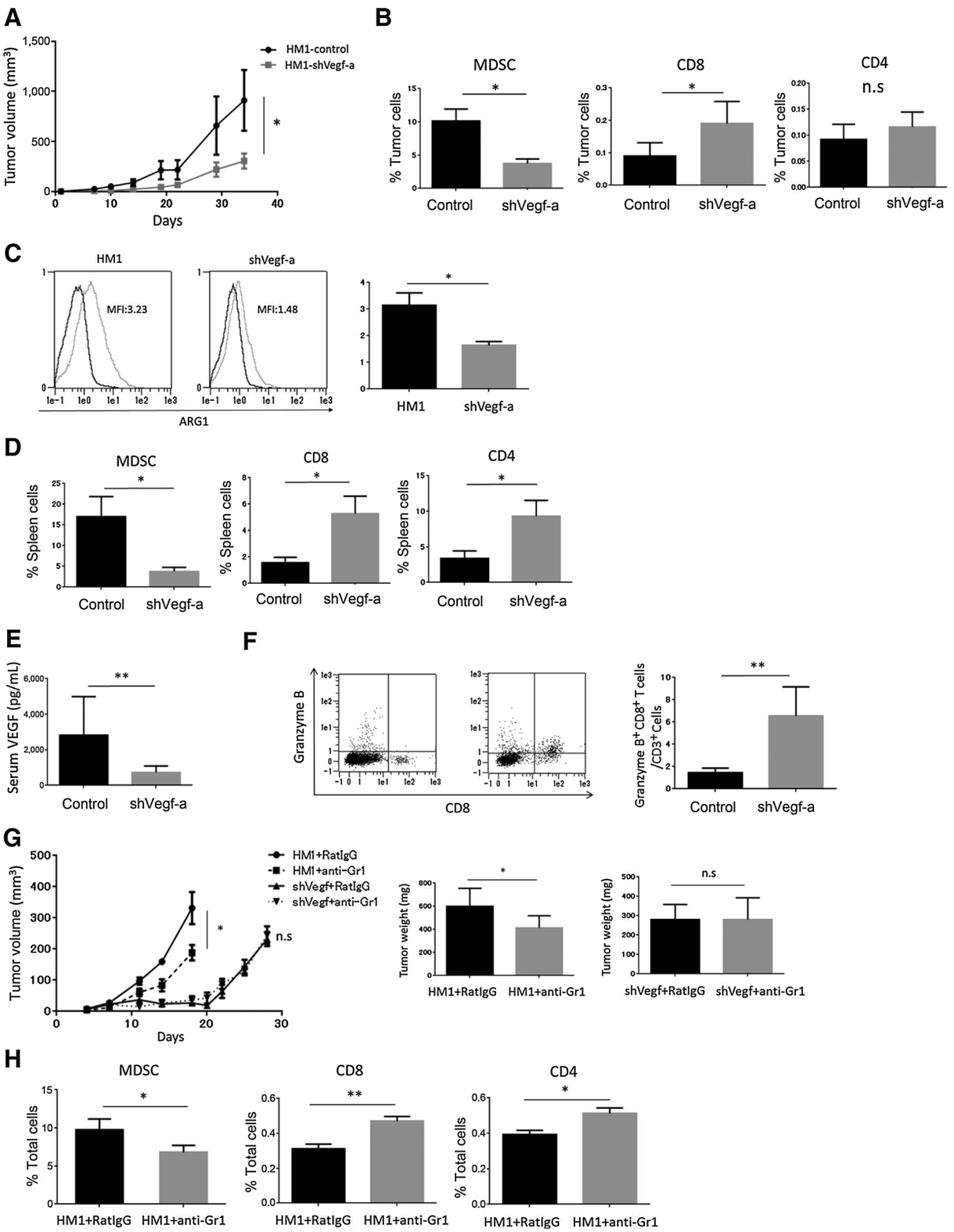

sh*Vegf-a* tumor-bearing mouse spleens were significantly increased compared with those in control tumor-bearing mice ($P < 0.05$; Fig. 5D), in which serum VEGF levels were significantly higher (2,820.6 vs. 732.5 pg/mL, respectively; $P < 0.005$; Fig. 5E). Splenic granzyme $B^+$ $CD8^+$ cells were also significantly increased in sh*Vegf-a* mice ($P < 0.005$; Fig. 5F), suggesting that tumor cell–secreted VEGF systemically inhibited $CD8^+$ T-cell function through MDSC induction. Intratumoral $Gr\text{-}1^+$ cell reduction via anti-Gr-1 Ab treatment modestly reduced the HM-1 control but not HM-1*shVegf-a* tumor burden ($P < 0.05$; Fig. 5G and Supplementary Fig. S7A and S7B). $CD8^+$ and $CD4^+$ cell frequencies were increased in anti-Gr-1 Ab–treated HM-1 tumors ($P < 0.05$, $P < 0.01$, respectively; Fig. 5H).

Taken together, these findings indicated that VEGF-A suppressed CTL functions through induction of MDSCs and promoted tumor progression.

## Discussion

VEGF expression in ovarian cancer has been shown to promote tumor angiogenesis and to be a poor prognostic factor (17), although its impact on other tumor microenvironment properties has not been fully elucidated. In the current study, clinical samples with high VEGF expression exhibited characteristics of immunosuppression via suppression of lymphocyte-related signals. Several molecular studies and histopathologic analyses of HGSOC have revealed that the "immunoreactive subtype", or cases with high lymphocyte infiltration, is associated with favorable prognosis, indicating that tumor immunity plays an important role in ovarian cancer progression (12, 13). In our study, the immunoreactive subtype showed a low VEGF signature score as determined by ssGSEA. Moreover, bevacizumab has recently been shown not to improve the outcomes of immunoreactive subtype cases, implying that the VEGF level contributes to the bevacizumab response. Unsupervised clustering analysis of triple-negative breast cancer showed an inverse correlation between VEGF and T-cell–related metagene expression (35), consistent with our data. In ovarian cancer, VEGF has been shown to suppress T-cell function directly (36), or through combination with COX1/COX2 by upregulating FasL on the endothelium (37). Consistent with this, our data demonstrated the upregulation of several MDSC chemoattractants in the VEGF-high group, indicating that the VEGF-associated immunosuppressive condition was primarily mediated through MDSC infiltration.

MDSCs promote tumor growth, tumor survival, and treatment resistance in many types of cancer (7) and express different surface markers depending on the cancer types (38). CD33 is broadly expressed on myeloid lineage cells; however, few reports have focused on $CD33^+$ cell infiltration in solid tumors. $CD33^+$ cell infiltration contributes to tumor progression in ovarian tumors by regulating ovarian cancer cell stemness (39) and predicts a poor prognosis in patients with prostate cancer (40). Here, we confirmed the inverse correlation between $CD33^+$ and $CD8^+$ cell infiltration within peritoneal dissemination, indicating the immunosuppressive properties of $CD33^+$ cells as MDSCs. Accordingly, $CD33^+$ cells isolated from patient ascites expressed ARG1 and inhibited $CD8^+$ T-cell proliferation. Human MDSCs are defined as $CD11b^+$ $CD33^+$ HLA-DR low $LIN^-$ cells (22, 23); however, we confirmed that $CD11b^+$ $CD33^+$ $LIN^-$ cells in ascites expressed ARG1, regardless of whether HLA-DR was expressed (Supplementary Fig. S2G). Moreover, in a previous study, $CD45^+$ $CD33^+$ $LIN^-$ cells in ovarian cancer were shown to express moderate levels of HLA-DR and to have immunosuppressive ability (39).

In this study, we demonstrated the correlation between VEGF expression in HGSOC peritoneal dissemination and $CD33^+$ MDSC infiltration, providing evidence for the immunosuppressive state and contributing to the poor prognosis. To the best of our knowledge, this is the first report to demonstrate the correlation of MDSCs with VEGF expression and $CD8^+$ cells in the tumor microenvironment. A study by Nakamura and colleagues suggested that there was an association between serum VEGF levels and systemic MDSC expansion (41). In this study, patients with strong infiltration of MDSCs in peritoneal dissemination, but not in the primary tumor, showed poor prognosis, and we did not find correlations in VEGF expression or $CD33^+$ cell number between primary and metastatic sites. A previous report showed that gene expression profiles of ovarian cancer tissues were different between primary and metastatic sites (42). Thus, we presumed that peritoneal dissemination expansion more directly affected patient prognosis, and that the omentum, the site most commonly involved in peritoneal dissemination, was a representative lymphatic organ that might be more susceptible to changes in the immune systems when constituting a tumor microenvironment. We have shown that immunosuppressive TGFβ signaling is also more active in peritoneal dissemination than in the primary site (43) and that an immune checkpoint molecule, PD-L1, is expressed in ovarian cancer peritoneal dissemination (11). Thus, VEGF and MDSCs in peritoneal dissemination play an important role in ovarian cancer progression.

*Vegf-a*–silenced tumor cells were shown to acquire immunogenicity through dendritic cell functional recovery (44), whereas VEGF inhibited dendritic cell maturation and recruited regulatory T cells and tumor-associated macrophages (19, 45). $CD11b^+$



**Figure 5.**

VEGF-A secreted by tumors induced MDSCs in spleens and tumors, and promoted tumor progression. **A,** Growth of subcutaneous HM-1 control or HM-1 sh*Vegf-a* tumors. The HM-1 control (black line) showed the fastest tumor growth, while growth was abrogated in HM-1 sh*Vegf-a* tumors (gray line; $n = 5$, *, $P < 0.05$). **B,** Proportions of $CD4^+$ cells, $CD8^+$ cells, and $CD11b^+Gr1^+$ cells in tumor cells. *, $P < 0.05$. **C,** ARG1 expression in MDSCs in HM-1 control tumors and sh*Vegf-a* tumors. The black line shows the isotype control; the gray line shows $ARG1^+$ cells. *, $P < 0.05$. **D,** Proportions of $CD4^+$ cells, $CD8^+$ cells, and $CD11b^+Gr1^+$ cells in the spleen cells. *, $P < 0.05$. **E,** Serum VEGF levels of the blood from tumor-bearing mice. Samples were collected at day 34 after tumor inoculation. **, $P < 0.01$. **F,** Flow cytometric analysis of granzyme $B^+$ $CD8^+$ cells in the spleen cells from tumor-bearing mice 72 hours after CD3/CD28 stimulation *in vitro*. **, $P < 0.01$. **G,** *In vivo* treatment of HM-1 control or HM-1 sh*Vegf-a* subcutaneous tumors with anti-Gr-1 antibody or Rat IgG as a control ($n = 5$). Anti-Gr-1 antibody was administered 150 μg/mouse intraperitoneally twice a week from 4 days after tumor inoculation. HM-1 control tumors were collected at day 18, while sh*Vegf-a* tumors were collected at day 28, when the average diameter of tumors reached more than 10 mm. *, $P < 0.05$. Tumor weights were also measured at the tumor collection day by digital scales. **H,** Frequencies of MDSCs, $CD8^+$ cells, and $CD4^+$ cells in HM-1 control tumors. *, $P < 0.05$; **, $P < 0.01$.

$Gr1^+$MDSCs were also shown to expand via VEGF signaling (19, 26) in cancer-free mice. To clarify the immunosuppressive mechanism of tumor-secreted VEGF, we demonstrated that tumor-secreted VEGF-A induced MDSCs in tumor sites and reduced intratumoral $CD8^+$ cells in two different mouse ovarian cancer models. To examine the impact of VEGF on MDSC functions, we confirmed the expression of VEGFR1 and VEGFR2 on MDSCs in tumors. $VEGFR2^+$ but not $VEGFR1^+$ MDSC frequencies were increased in tumors, indicating the differential effects of these receptors on MDSC function. Huang and colleagues showed that VEGFR2 signaling but not VEGFR1 signaling induced systemic MDSC expansion (20). In addition, we showed that $VEGFR2^+$ MDSC frequencies were higher in ARG1-expressing than in ARG1-negative MDSCs, indicating that $VEGFR2^+$ MDSCs exhibited stronger immunosuppressive properties in tumors. VEGF/VEGFR2 signaling also directly promoted MDSC differentiation and migration. Therefore, the VEGF/VEGFR2 axis might directly recruit MDSCs to tumors sites and inhibit T-cell function. A study of endothelial cells demonstrated that an interaction between a hypoxia-driven VEGF/VEGFR autocrine loop and hypoxia-inducible factor (HIF)-1α (46). Similar mechanisms might influence VEGFR expression on intratumoral MDSCs. Indeed, hypoxic condition has been shown to upregulate ARG1 expression in MDSCs (47). Thus, the immunosuppressive properties of hypoxia/VEGF-induced MDSC subpopulations might be particularly strong, although further studies are required to confirm this hypothesis.

In the HM-1 mouse model, the numbers of MDSCs were increased in both the spleen and tumor compared with those in sh*Vegf-a* tumor-bearing mice, and serum VEGF levels reflected those in the tumor. A previous study showed that VEGF concentrations in CT26 murine colon tumors expressing VEGF-A were over 10-fold higher than plasma levels (48), suggesting that MDSCs generated in the bone marrow effluent into the blood stream and are then recruited to the tumor microenvironment in accordance with the VEGF level.

In this study, we found that the therapeutic effects of intratumoral MDSC reduction via an anti-Gr-1 Ab treatment were abrogated by VEGF silencing. Several reports have demonstrated the antitumor effects of anti-Gr-1 Abs via enhancement of immune response (33), although anti-Gr-1 Abs alone are not effective against EL4 and LLC tumors (49) and the immunosuppressive functions of $CD11b^+Gr1^+$ cells in tumors differ among tumor types (6). Our data indicated that the therapeutic effects of anti-Gr-1 Abs were affected by the concentration of VEGF in the tumor. Thus, suppression of VEGF signal might enhance tumor immunity by inhibiting MDSC expansion. The clinical benefit in combination of dendritic cell vaccination and bevacizumab for recurrent ovarian cancer has been reported (50). Accordingly, targeting VEGF signal may improve the efficacy of various immunotherapies.

In summary, we showed that high expression of VEGF in ovarian cancer recruited MDSCs to the tumor and inhibited tumor immunity. Treatments targeting MDSCs induced by VEGF signaling may improve prognoses in patients with HGSOC.

## Disclosure of Potential Conflicts of Interest

J. Hamanishi reports receiving commercial research grants from Daiichi Sankyo, Japan. No potential conflicts of interest were disclosed by the other authors.

## Authors' Contributions

**Conception and design:** N. Horikawa, K. Abiko, N. Matsumura, J. Hamanishi, T. Baba, I. Konishi
**Development of methodology:** N. Horikawa, K. Abiko, T. Baba
**Acquisition of data (provided animals, acquired and managed patients, provided facilities, etc.):** N. Horikawa, K. Abiko
**Analysis and interpretation of data (e.g., statistical analysis, biostatistics, computational analysis):** N. Horikawa, T. Baba, K. Yamaguchi, I. Konishi
**Writing, review, and/or revision of the manuscript:** N. Horikawa, K. Abiko, N. Matsumura, T. Baba, K. Yamaguchi, Y. Yoshioka
**Administrative, technical, or material support (i.e., reporting or organizing data, constructing databases):** N. Horikawa, K. Yamaguchi, M. Koshiyama
**Study supervision:** K. Abiko, N. Matsumura, M. Koshiyama, I. Konishi

## Acknowledgments

The authors thank Yuko Hosoe for her excellent technical assistance.

## Grant Support

This work was supported by a Grant-in-Aid for Scientific Research (KAKENHI) from the Ministry of Education, Culture, Sports, Science and Technology (MEXT; Nos. 50724390 and 20508246).

The costs of publication of this article were defrayed in part by the payment of page charges. This article must therefore be hereby marked *advertisement* in accordance with 18 U.S.C. Section 1734 solely to indicate this fact.

Received February 20, 2016; revised June 1, 2016; accepted June 17, 2016; published OnlineFirst July 11, 2016.

## References

1. Ebell MH, Culp MB, Radke TJ. A systematic review of symptoms for the diagnosis of ovarian cancer. Am J Prev Med 2016;50:384–94.
2. Vaughan S, Coward JI, Bast RC, Berchuck A, Berek JS, Brenton JD, et al. Rethinking ovarian cancer: recommendations for improving outcomes. Nat Rev Cancer 2011;11:719–25.
3. Coleman RL, Monk BJ, Sood AK, Herzog TJ. Latest research and treatment of advanced-stage epithelial ovarian cancer. Nat Rev Clin Oncol 2013; 10:211–24.
4. Hanahan D, Weinberg RA. Hallmarks of cancer: the next generation. Cell 2011;144:646–74.
5. Zou W. Regulatory T cells, tumour immunity and immunotherapy. Nat Rev Immunol 2006;6:295–307.
6. Holmgaard RB, Zamarin D, Li Y, Gasmi B, Munn DH, Allison JP, et al. Tumor-expressed IDO recruits and activates MDSCs in a Treg-dependent manner. Cell Rep 2015;13:1–13.
7. Gabrilovich DI, Nagaraj S. Myeloid-derived suppressor cells as regulators of the immune system. Nat Rev Immunol 2009;9: 162–74.
8. Qian B-Z, Pollard JW. Macrophage diversity enhances tumor progression and metastasis. Cell 2010;141:39–51.
9. Hamanishi J, Mandai M, Iwasaki M, Okazaki T, Tanaka Y, Yamaguchi K, et al. Programmed cell death 1 ligand 1 and tumor-infiltrating CD8+ T lymphocytes are prognostic factors of human ovarian cancer. Proc Natl Acad Sci U S A 2007;104:3360–5.
10. Abiko K, Mandai M, Hamanishi J, Yoshioka Y, Matsumura N, Baba T, et al. PD-L1 on tumor cells is induced in ascites and promotes peritoneal dissemination of ovarian cancer through CTL dysfunction. Clin Cancer Res 2013;19:1363–74.
11. Hamanishi J, Mandai M, Ikeda T, Minami M, Kawaguchi A, Murayama T, et al. Safety and antitumor activity of anti-PD-1 antibody, nivolumab, in

patients with platinum-resistant ovarian cancer. J Clin Oncol 2015;33:4015–22.
12. The Cancer Genome Atlas Research Network. Integrated genomic analyses of ovarian carcinoma. Nature 2011;474:609–15.
13. Murakami R, Matsumura N, Mandai M, Yoshihara K, Tanabe H, Nakai H, et al. Establishment of a novel histopathological classification of high-grade serous ovarian carcinoma correlated with prognostically distinct gene expression subtypes. Am J Pathol 2016;186:1103–13.
14. Tothill RW, Tinker AV, George J, Brown R, Fox SB, Lade S, et al. Novel molecular subtypes of serous and endometrioid ovarian cancer linked to clinical outcome. Clin Cancer Res 2008;14:5198–208.
15. Sato E, Olson SH, Ahn J, Bundy B, Nishikawa H, Qian F, et al. Intraepithelial CD8+ tumor-infiltrating lymphocytes and a high CD8+/regulatory T cell ratio are associated with favorable prognosis in ovarian cancer. Proc Natl Acad Sci U S A 2005;102:18538–43.
16. Zhang L, Conejo-Garcia JR, Katsaros D, Gimotty PA, Massobrio M, Regnani G, et al. Intratumoral T cells, recurrence, and survival in epithelial ovarian cancer. N Engl J Med 2003;348:203–13.
17. Yamamoto S, Konishi I, Mandai M, Kuroda H, Komatsu T, Nanbu K, et al. Expression of vascular endothelial growth factor (VEGF) in epithelial ovarian neoplasms: correlation with clinicopathology and patient survival, and analysis of serum VEGF levels. Br J Cancer 1997;76:1221–7.
18. Voron T, Marcheteau E, Pernot S, Colussi O, Tartour E, Taieb J, et al. Control of the immune response by pro-angiogenic factors. Front Oncol 2014;4:70.
19. Gabrilovich DI, Chen HL, Girgis KR, Cunningham HT, Meny GM, Nadaf S, et al. Production of vascular endothelial growth factor by human tumors inhibits the functional maturation of dendritic cells. Nat Med 1996;2:1096–103.
20. Solito S, Falisi E, Diaz-montero CM, Doni A, Pinton L, Francescato S, et al. A human promyelocytic-like population is responsible for the immune suppression mediated by myeloid-derived suppressor cells. Blood 2011;118:2254–65.
21. Montero AJ, Diaz-Montero CM, Kyriakopoulos CE, Bronte V, Mandruzzato S. Myeloid-derived suppressor cells in cancer patients: a clinical perspective. J Immunother 2012;35:107–15.
22. Greten TF, Manns MP, Korangy F. Myeloid derived suppressor cells in human diseases. Int Immunopharmacol 2011;11:802–7.
23. Lu R, Kujawski M, Pan H, Shively JE. Tumor angiogenesis mediated by myeloid cells is negatively regulated by CEACAM1. Cancer Res 2012;72:2239–50.
24. Toh B, Wang X, Keeble J, Sim WJ, Khoo K, Wong WC, et al. Mesenchymal transition and dissemination of cancer cells is driven by myeloid-derived suppressor cells infiltrating the primary tumor. PLoS Biol 2011;9:e1001162.
25. Talmadge JE, Gabrilovich DI. History of myeloid-derived suppressor cells. Nat Rev Cancer 2013;13:739–52.
26. Huang Y, Chen X, Dikov MM, Novitskiy SV, Mosse CA, Yang L, et al. Distinct roles of VEGFR-1 and VEGFR-2 in the aberrant hematopoiesis associated with elevated levels of VEGF. Blood 2007;110:624–31.
27. Barnett JC, Bean SM, Whitaker RS, Kondoh E, Baba T, Fujii S, et al. Ovarian cancer tumor infiltrating T-regulatory (T(reg)) cells are associated with a metastatic phenotype. Gynecol Oncol 2010;116:556–62.
28. Abiko K, Matsumura N, Hamanishi J, Horikawa N, Murakami R, Yamaguchi K, et al. IFN-$\gamma$ from lymphocytes induces PD-L1 expression and promotes progression of ovarian cancer. Br J Cancer 2015;1:1–9.
29. Choe SE, Boutros M, Michelson AM, Church GM, Halfon MS. Preferred analysis methods for Affymetrix GeneChips revealed by a wholly defined control dataset. Genome Biol 2005;6:R16.
30. Barbie DA, Tamayo P, Boehm JS, Kim SY, Moody SE, Dunn IF, et al. Systematic RNA interference reveals that oncogenic KRAS-driven cancers require TBK1. Nature 2009;462:108–12.
31. Hamanishi J, Mandai M, Matsumura N, Baba T, Yamaguchi K, Fujii S, et al. Activated local immunity by CCL19-transduced embryonic endothelial progenitor cells suppresses metastasis of murine ovarian cancer. Stem Cells 2010;28:164–73.
32. Roby KF, Taylor CC, Sweetwood JP, Cheng Y, Pace JL, Tawfik O, et al. Development of a syngeneic mouse model for events related to ovarian cancer. Carcinogenesis 2000;21:585–91.
33. Chang SH, Mirabolfathinejad SG, Katta H, Cumpian AM, Gong L, Caetano MS, et al. T helper 17 cells play a critical pathogenic role in lung cancer. Proc Natl Acad Sci U S A 2014;111:1–6.
34. Ren J-G, Seth P, Clish CB, Lorkiewicz PK, Higashi RM, Lane AN, et al. Knockdown of malic enzyme 2 suppresses lung tumor growth, induces differentiation and impacts PI3K/AKT signaling. Sci Rep 2014;4:5414.
35. Rody A, Karn T, Liedtke C, Pusztai L, Ruckhaeberle E, Hanker L, et al. A clinically relevant gene signature in triple negative and basal-like breast cancer. Breast Cancer Res 2011;13:R97.
36. Gavalas NG, Tsiatas M, Tsitsilonis O, Politi E, Ioannou K, Ziogas AC, et al. VEGF directly suppresses activation of T cells from ascites secondary to ovarian cancer via VEGF receptor type 2. Br J Cancer 2012;107:1869–75.
37. Gregory TM, Stephen PS, Li-Ping W, Tom G, Ricardo RL, Ian SH, et al. Tumor endothelium FasL establishes a selective immune barrier promoting tolerance in tumor. Nature 2014;20:607–15.
38. Solito S, Marigo I, Pinton L, Damuzzo V, Mandruzzato S, Bronte V. Myeloid-derived suppressor cell heterogeneity in human cancers. Ann N Y Acad Sci 2014;1319:47–65.
39. Cui TX, Kryczek I, Zhao L, Zhao E, Kuick R, Roh MH, et al. Myeloid-derived suppressor cells enhance stemness of cancer cells by inducing microRNA101 and suppressing the corepressor CtBP2. Immunity 2013;39:611–21.
40. Di Mitri D, Toso A, Chen JJ, Sarti M, Pinton S, Jost TR, et al. Tumour-infiltrating Gr-1+ myeloid cells antagonize senescence in cancer. Nature 2014;515:134–7.
41. Nakamura I, Shibata M, Gonda K, Yazawa T, Shimura T, Anazawa T, et al. Serum levels of vascular endothelial growth factor are increased and correlate with malnutrition, immunosuppression involving MDSCs and systemic inflammation in patients with cancer of the digestive system. Oncol Lett 2013;5:1682–6.
42. Eliana B, Renata AT, Stefano C, Antonella R, Elisabetta B, Elisa R, et al. Gene expression profile of ovarian serous papillary carcinomas: identification of metastasis-associated genes. Am J Obstet Gynecol 2007;196:1–11.
43. Yamamura S, Matsumura N, Mandai M, Huang Z, Oura T, Baba T, et al. The activated transforming growth factor-beta signaling pathway in peritoneal metastases is a potential therapeutic target in ovarian cancer. Int J Cancer 2012;130:20–8.
44. Shi Y, Yu P, Zeng D, Qian F, Lei X, Zhao Y, et al. Suppression of vascular endothelial growth factor abrogates the immunosuppressive capability of murine gastric cancer cells and elicits antitumor immunity. FEBS J 2014;281:3882–93.
45. Terme M, Pernot S, Marcheteau E, Sandoval F, Benhamouda N, Colussi O, et al. VEGFA-VEGFR pathway blockade inhibits tumor-induced regulatory T-cell proliferation in colorectal cancer. Cancer Res 2013;73:539–49.
46. Tang N, Wang L, Esko J, Giordano FJ, Huang Y, Gerber HP, et al. Loss of HIF-1alpha in endothelial cells disrupts a hypoxia-driven VEGF autocrine loop necessary for tumorigenesis. Cancer Cell 2004;6:485–95.
47. Cesar AC, Thomas C, Lily L, Matthew JC, Je-In Y, Pingyan C, et al. HIF-1a regulates function and differentiation of myeloid-derived suppressor cells in the tumor microenvironment. J.Exp.Med 2010;207:2439–53.
48. Voron T, Colussi O, Marcheteau E, Pernot S, Nizard M, Pointet A-L, et al. VEGF-A modulates expression of inhibitory checkpoints on CD8+ T cells in tumors. J Exp Med 2015;212:139–48.
49. Shojaei F, Wu X, Malik AK, Zhong C, Baldwin ME, Schanz S, et al. Tumor refractoriness to anti-VEGF treatment is mediated by CD11b+Gr1+ myeloid cells. Nat Biotechnol 2007;25:911–20.
50. Lana EK, Daniel JP, Cheryl LC, Janos T, Sarah K, Marnix B, et al. Autologous lysate-pulsed dendritic cell vaccination followed by adoptive transfer of vaccine-primed ex vivo co-stimulated T cells in recurrent ovarian cancer. Oncoimmunol 2013;2:e22664.